

Shadow-Feature-Enhanced ML-CFAR Detection for a Swerling 1 Target in Weibull Clutter

J. W. Minett, S. W. Leung, Y. M. Siu, and M. K. Lee

Department of Electronic Engineering
City University of Hong Kong
Tat Chee Avenue
Kowloon, Hong Kong

Abstract—This paper describes a shadow-feature-enhanced technique for the Maximum-Likelihood CFAR (ML-CFAR) detector, which is known to have a low CFAR loss. Detection enhancement for a shadow length of 5 bins is obtained for a Swerling 1 target in Weibull clutter for signal-to-clutter ratio lower than about 12 dB.

I. INTRODUCTION

The shadow feature (or shadowing) is observed in some radar detection scenarios when an object that lies within the main beam of the antenna screens a region of the detection space, often at low grazing angle. Objects that lie within the screened area reflect little or no energy back to the radar receiver. When rough terrain, for example, causes shadowing, a target located within the shadow may be rendered invisible to the radar, causing a reduction in detection performance. The effects of such kinds of shadowing have been studied by Smith [1], Sancer [2], and others. However, when a target screens a region of clutter, the resultant drop in mean clutter power received from the screened region may allow the target to be detected more easily. Only a few papers [3, 4] have appeared recently that discuss this phenomenon.

The maximum-likelihood constant false alarm rate (ML-CFAR) detector is known to have low CFAR loss for Weibull background [5]. In the following sections, a shadow-feature-

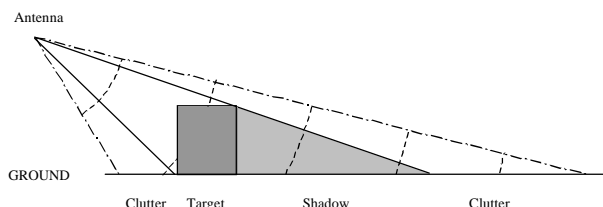
enhanced detector is described and analyzed for a Swerling 1 target in Weibull clutter using ML-CFAR detection [5] in the test bin and adapted ML-CFAR detection in each of the shadow bins to detect the shadow.

II. MODELING THE SHADOW FEATURE

A simplified illustration of the shadow feature induced by a ground-based target is shown in Fig. 1. Clutter is received from the bins preceding and, perhaps, some of the bins trailing the test bin (target bin); we call these bins *clutter bins* and, collectively, the *clutter window*. However, no clutter is received from the bins immediately trailing the target due to the target screening them; we call these bins *shadow bins* and, collectively, the *shadow window*. The idea behind shadow-feature-enhanced detection is to detect the shadow feature rather than the target itself. When a shadow is detected with sufficiently high probability, the presence of a target is inferred. In regions of high clutter power, it will often be far easier to detect the shadow bins, which contain noise only. We assume that clutter cannot induce a shadow feature and that there is no sidelobe clutter or other source of interference.

Fig. 2 shows the layout of the detection window when no target is present. Fig. 3 shows the layout of the detection window when a target is present in the test bin. In particular, the latter figure shows the induced shadow feature, whose bins contain noise only, trailing the target.

We shall now investigate the details of the shadow-feature-enhanced detection technique. Detection is performed in both the test bin and in the shadow bins trailing the test bin. Detection in the test bin is carried out in the normal way; in Section III we shall use ML-CFAR detection, which has low



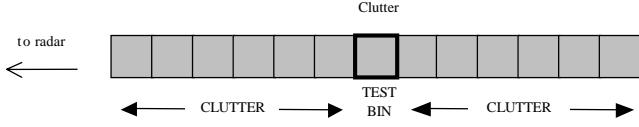


Fig. 2. Layout of the detection window for no target present.

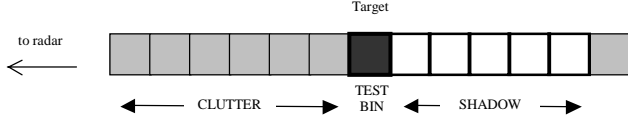


Fig. 3. Layout of the detection window for target present.

CFAR loss [5]. Denoting the “No Target Present” hypothesis by H_0 and the “Target Present” hypothesis by H_1 , the hypotheses tested in the test bin are

$$\begin{aligned} H_0 : \text{ReceivedSignal} &= \text{Clutter} + \text{Noise}, \\ H_1 : \text{ReceivedSignal} &= \text{Target} + \text{Clutter} + \text{Noise}. \end{aligned} \quad (1)$$

The total return in the test bin is denoted by x ; the returns in the shadow bins are denoted by $y_i : i=1, \dots, l$, where l is the length of the shadow window; and the clutter (plus noise) returns in the clutter bins are denoted by $z_j : j=1, \dots, p$, where p is the size of the clutter window. The decision rule we use in the test bin is of the same form as that used by Ravid and Levanon [5],

$$x \begin{cases} \geq \\ < \end{cases} \begin{matrix} H_1 \\ H_0 \end{matrix} T(\mathbf{z}), \quad (2)$$

where $T(\mathbf{z})$ is an adaptive threshold for constant false alarm rate control. Thus hypothesis H_1 is selected when the test bin return, x , exceeds the threshold, T .

Detection is also performed in each of the shadow bins where we test the hypotheses

$$\begin{aligned} H_0 : \text{ReceivedSignal} &= \text{Clutter} + \text{Noise}, \\ H_1 : \text{ReceivedSignal} &= \text{Noise}. \end{aligned} \quad (3)$$

When the target signal is present in the test bin, under H_1 , the shadow bin returns consist of noise only, which we assume to have much lower power than the clutter bin returns. Detection in the shadow bins is therefore carried out by the decision rule

$$y_i \begin{cases} < \\ \geq \end{cases} \begin{matrix} H_1 \\ H_0 \end{matrix} k T(\mathbf{z}), \quad (4)$$

where $T(\mathbf{z})$ is the same adaptive threshold as in the test bin

decision rule (2) and $k \in [0, 1]$ is a factor that allows the shadow bin threshold to be varied independently. Thus hypothesis H_1 is selected when the shadow bin return, y_i , is **lower** than the threshold, kT .

The detection decisions in the individual bins are combined to form a global decision rule: a target is detected only when hypothesis H_1 is selected in the test bin and in each of the shadow bins. We denote the false alarm and detection rate in the test bin by P_t^F and P_t^D , and in each shadow bin by P_s^F and P_s^D , respectively. The false alarm and detection rates of the shadow-feature-enhanced detector are therefore given by $P^F = P_t^F (P_s^F)^l$ and $P^D = P_t^D (P_s^D)^l$, respectively.

III. SHADOW FEATURE ENHANCED ML-CFAR DETECTION OF A SWERLING 1 TARGET IN WEIBULL CLUTTER

In this section, we apply the model discussed in Section II to enhance the performance of the ML-CFAR detector for a Swerling 1 target in Weibull clutter. Ravid and Levanon have analyzed the performance of this ML-CFAR detector [5] without shadow feature enhancement.

The distributions of the signal returns in the detection window under each hypothesis are modeled as shown in Table 1; $W(b, c)$ denotes a Weibull variate with unknown scale parameter b and known shape parameter c , and $R(b)$ denotes a Rayleigh variate with scale parameter b . Note in particular that the test bin returns under H_1 are modeled as the vector sum of a Weibull variate (the clutter) and a Rayleigh variate (the Swerling 1 target).

TABLE I
DISTRIBUTION OF SIGNAL RETURNS UNDER H_0 AND H_1

	H_0	H_1
Test Bin	$X \sim W(b, c)$	$X \sim W(b, c) \oplus R(b_t)$
Shadow Bins	$Y_i \sim W(b, c)$	$Y_i \sim R(b_n)$
Clutter Bins	$Z_j \sim W(b, c)$	$Z_j \sim W(b, c)$

Ravid and Levanon construct an adaptive threshold in the test bin [5],

$$T(\mathbf{z}) = \alpha \hat{b}, \quad (5)$$

where \hat{b} is the maximum-likelihood estimate of the clutter scale parameter, b , for Weibull clutter with known shape parameter, c . Combining (4) and (5), the threshold set in the shadow window bins is

$$T'(\mathbf{z}) := k\alpha\hat{b}. \quad (6)$$

The false alarm rate of the detector is obtained by calculating the probability that hypothesis H_1 is selected when no target is present. H_1 is selected only when a target is detected in the test bin, according to decision rule (2), **and** the shadow feature is detected in each shadow window bin, according to decision rule (4). The false alarm rate in the test bin only is [5]

$$P_i^F = \left(1 + \frac{\alpha^c}{p}\right)^{-p}. \quad (7)$$

We can show, in a similar manner, that the false alarm rate in each shadow bin is [6]

$$P_s^F = 1 - \left[1 + \frac{(k\alpha)^c}{p}\right]^{-p}, \quad (8)$$

Consequently, the false alarm rate of the shadow-feature-enhanced ML-CFAR detector is

$$P^F = \left[1 + \frac{\alpha^c}{p}\right]^{-p} \left\{1 - \left[1 + \frac{(k\alpha)^c}{p}\right]^{-p}\right\}^l, \quad (9)$$

which does not depend on the clutter scale parameter, b , indicating that the detector is CFAR.

The detection rate is derived similarly. Ravid and Levanon obtain an approximate expression (exact for Rayleigh clutter, $c = 2$) for the detection rate in the test bin [5]

$$P_i^D = \left[1 + \frac{\alpha^2}{p(1+SCR)}\right]^{-p}, \quad (10)$$

where SCR is the signal-to-clutter ratio defined by

$$SCR := \frac{b_i^2}{b^2 \Gamma(1 + \frac{2}{c})}. \quad (11)$$

We can also show that the detection rate in each shadow bin is approximately (exact for $c = 2$)

$$P_s^D = 1 - \left[1 + \frac{(k\alpha)^2 CNR}{p}\right]^{-p}, \quad (12)$$

where CNR is the clutter-to-noise ratio defined by

$$CNR := \frac{b^2 \Gamma(1 + \frac{2}{c})}{b_n^2}. \quad (13)$$

Consequently, the detection rate of the shadow-feature-enhanced ML-CFAR detector is approximately

$$P^D = \left[1 + \frac{\alpha^2}{p(1+SCR)}\right]^{-p} \left\{1 - \left[1 + \frac{(k\alpha)^2 CNR}{p}\right]^{-p}\right\}^l. \quad (14)$$

Fig. 4 shows a plot of receiver operating characteristics of the detector for several values of the shadow length, l , at SCR 0dB and CNR 10dB. The curve for $l = 0$ corresponds to the ROC for the standard ML-CFAR detector. For large threshold values (the lower portions of the curves) and $l = 3$ or 5 , the performance of the shadow-feature-enhanced detector is close to that of the standard ML-CFAR detector. At a certain value of α , the false alarm rate reaches a maximum value well below 1.0, beyond which it falls back towards zero. However, the detection rate continues to rise close to 1.0 before it too starts to fall. For example, at false alarm rate 10^{-4} , the ML-CFAR detector achieves detection rate of about 10^{-3} whereas the shadow-feature-enhanced detector achieves detection rate above 10% for shadow length $l = 3$. This is because, although the threshold has been lowered to improve the overall detection rate, the shadow feature algorithm has compensated for the undesirable increase in the ML-CFAR false alarm rate in just the test bin, resulting in better overall performance. This phenomenon can also be observed in (9).

Fig. 5 shows a plot of the detection rate against signal-to-clutter ratio. The graph indicates that for shadow length $l = 5$ at false alarm rate 10^{-6} and clutter-to-noise ratio 10dB, the detection rate is essentially independent of the signal-to-

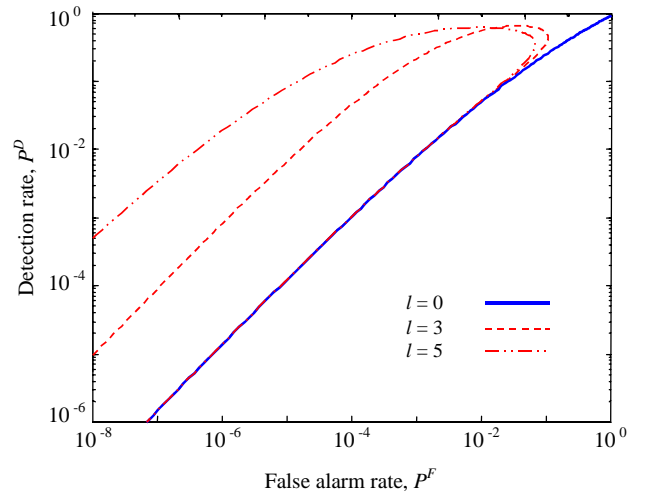


Fig. 4. Receiver operating characteristics for various values of l ($p = 4$; $l = 0, 3, 5$; $SCR = 0$ dB; $CNR = 10$ dB; $k = 1$).

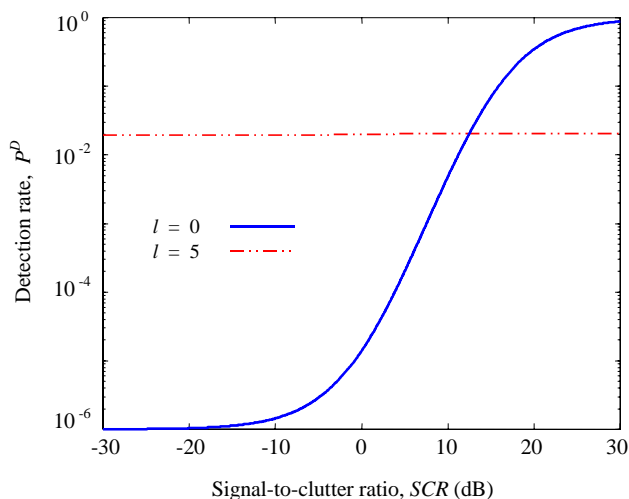


Fig. 5. Plot of the detection rate against signal-to-clutter ratio ($p = 4$; $l = 0, 5$; $CNR = 10$ dB; $k = 1$).

clutter ratio. Detection enhancement results for signal-to-clutter ratio **less than** about 12 dB. Since we would typically be interested in detecting signals weaker than 12 dB, this threshold signal-to-clutter ratio is not restrictive.

IV. CONCLUSION

We have demonstrated a method for enhancing detection performance when a shadow feature occurs. The method has been applied to enhance ML-CFAR detection for a Swerling 1 target in Weibull clutter. Results demonstrate that when the shadow feature of length 5 bins occurs at clutter-to-noise ratio 10 dB, detection enhancement can be achieved for signal-to-clutter ratio **lower than** 12 dB. The detection rate is essentially independent of the signal-to-clutter ratio at low false alarm rates such as 10^{-6} .

REFERENCES

- [1] B. G. Smith, "Geometrical Shadowing of a random rough surface," IEEE Trans. Ant. Prop., 15(5), 1967, pp. 668-671.
- [2] M. I. Sancer, "Shadow-corrected electromagnetic scattering from a randomly rough surface," IEEE Trans. Ant. Prop., 17(5), 1969, pp. 577-585.
- [3] S. W. Leung, K. H. Yeung, T. W. S. Chow, & P. W. Tse, "Shadow feature enhancement in radar detection," Proc. ISITA '90, Hawaii, U.S.A., November 27-30, 1990.
- [4] S. W. Leung, J. W. Minett, & C. F. Chung, "An analysis of the shadow feature technique in radar detection," IEEE Trans. Aero. Elec. Sys., 35(3), 1999, pp. 1104-1106.
- [5] R. Ravid and N. Levanon, "Maximum-likelihood CFAR for Weibull background," IEE Proc.-F, 139(3), 1992, pp. 256-264.